

## SUPPLEMENTARY INFORMATION

### Unveiling Structural Defects by $^{139}\text{La}$ NMR and Raman Spectroscopies at the Origin of Surface Stability for the Design of Cerium-Based Catalyst

Rémy Pointecouteau<sup>1,2</sup>, Pierre Florian<sup>3</sup>, Vincent Rodriguez<sup>4</sup>, Nicolas Bion<sup>2</sup> and Alain Demourgues<sup>1\*</sup>

1. CNRS, University of Bordeaux, Bordeaux INP, ICMCB UMR CNRS 5026, F-33600, Pessac, France

2. CNRS, University of Poitiers, IC2MP UMR CNRS 7285, F-86000, Poitiers, France

3. CNRS, UPR CNRS 3079 CEMHTI, F-45100, Orléans, France

4. Institut des Sciences Moléculaires, UMR 5255 CNRS, Université de Bordeaux, 351 Cours de la Libération, F-33405 Talence Cedex, France

## FIGURE CAPTION

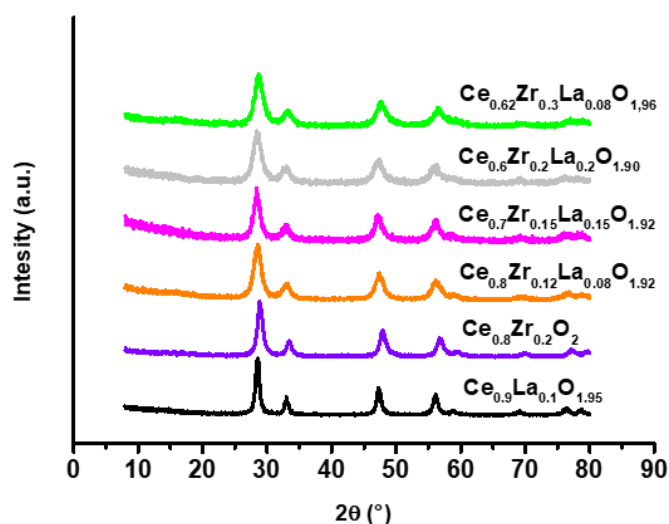


Figure 1-SI: Powder XRD patterns of  $\text{Ce}_{1-x-y}\text{Zr}_x\text{La}_y\text{O}_{2-z}$  complex oxides annealed at  $600^\circ\text{C}$  under air

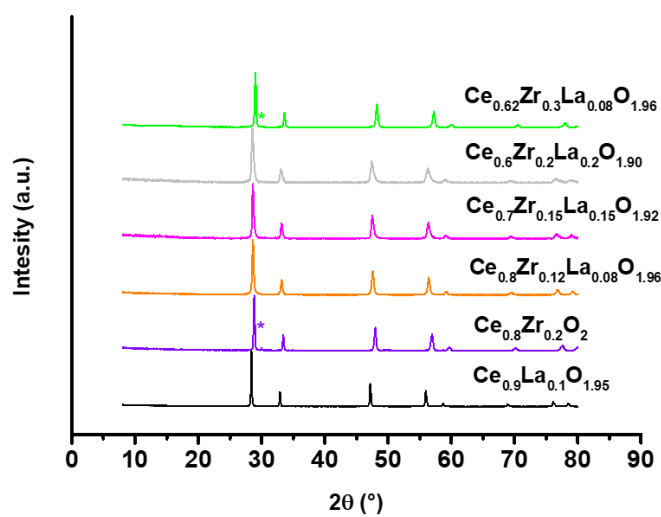
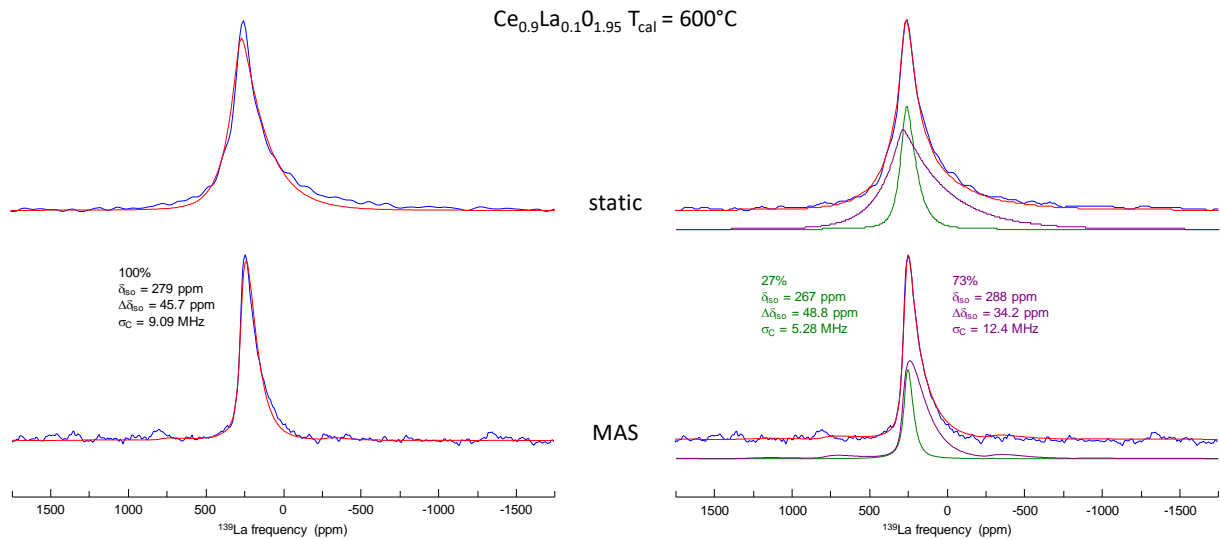
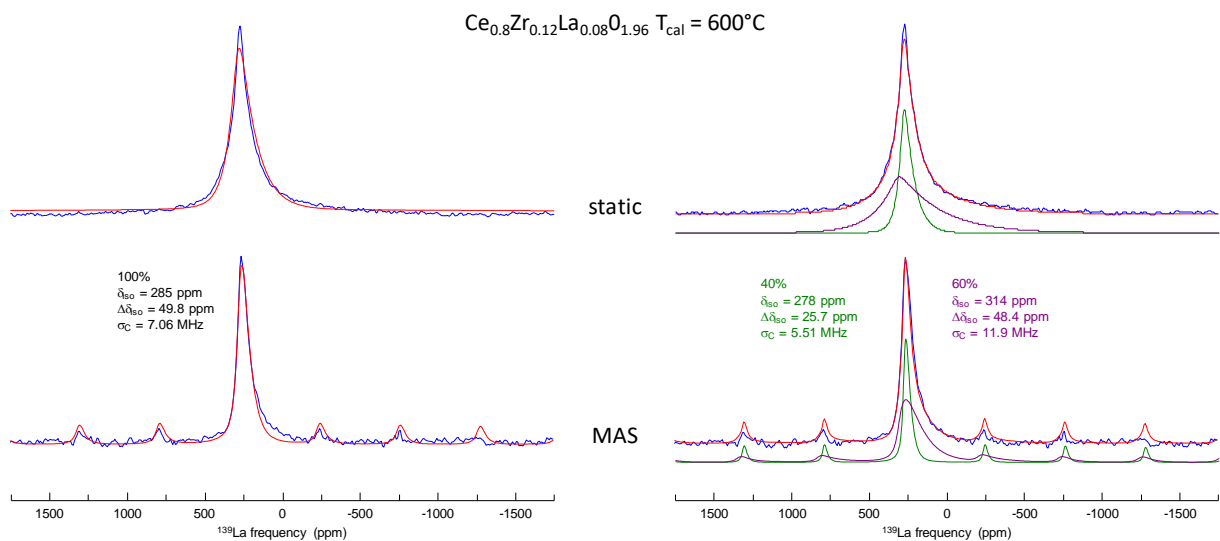


Figure 2-SI: Powder XRD patterns of  $\text{Ce}_{1-x-y}\text{Zr}_x\text{La}_y\text{O}_{2-z}$  complex oxides annealed at  $1200^\circ\text{C}$  under air



*Figure 3-SI:* Comparison of the best fit simulations of the  $^{139}\text{La}$  NMR spectra of  $\text{Ce}_{0.9}\text{La}_{0.1}\text{O}_{1.95}$  annealed at  $600^\circ\text{C}$  and using one- (left) and two- (right) Czjzek-like components. Simulations account simultaneously for the static (top) and spinning (bottom) experimental spectra.



*Figure 4-SI:* Comparison of the best fit simulations of the  $^{139}\text{La}$  NMR spectra of  $\text{Ce}_{0.8}\text{Zr}_{0.12}\text{La}_{0.08}\text{O}_{1.96}$  annealed at  $600^\circ\text{C}$  and using one- (left) and two- (right) Czjzek-like components. Simulations account simultaneously for the static (top) and spinning (bottom) experimental spectra.

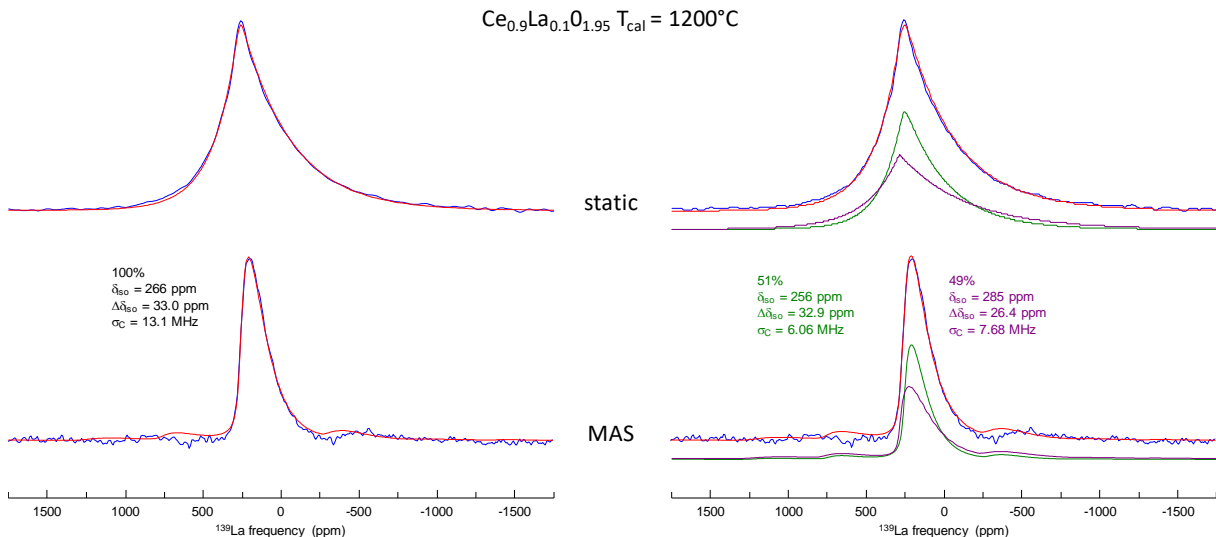


Figure 5-SI: Comparison of the best fit simulations of the  $^{139}\text{La}$  NMR spectra of  $\text{Ce}_{0.9}\text{La}_{0.1}\text{O}_{1.95}$  annealed at  $1200^\circ\text{C}$  and using one- (left) and two- (right) Czjzek-like components. Simulations account simultaneously for the static (top) and spinning (bottom) experimental spectra.

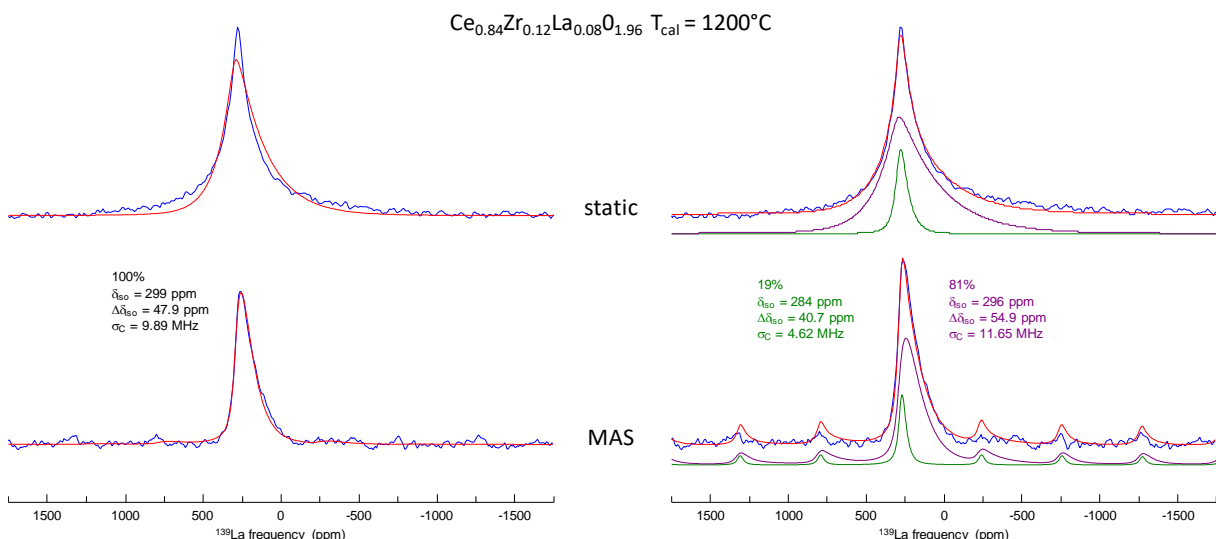


Figure 6-SI: Comparison of the best fit simulations of the  $^{139}\text{La}$  NMR spectra of  $\text{Ce}_{0.84}\text{Zr}_{0.12}\text{La}_{0.08}\text{O}_{1.96}$  annealed at  $1200^\circ\text{C}$  and using one- (left) and two- (right) Czjzek-like components. Simulations account simultaneously for the static (top) and spinning (bottom) experimental spectra.

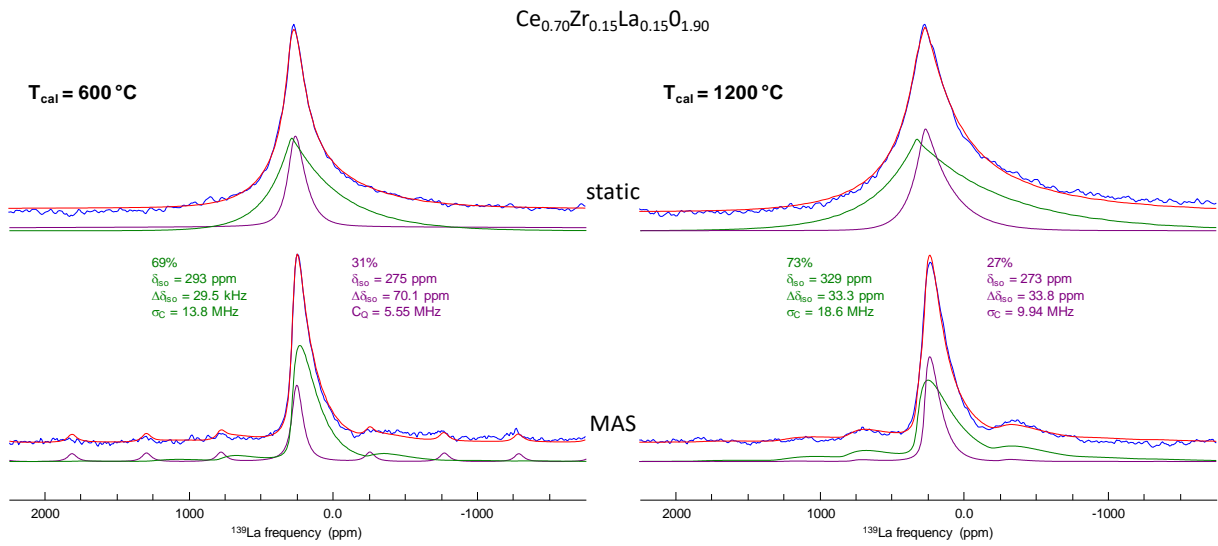


Figure 7-SI: Best fit simulations of the  $^{139}\text{La}$  NMR spectra of  $\text{Ce}_{0.70}\text{Zr}_{0.15}\text{La}_{0.15}\text{O}_{1.90}$  annealed at  $600^\circ\text{C}$  (left) and  $1200^\circ\text{C}$  (right) and using two Czjzek-like components. Simulations account simultaneously for the static (top) and spinning (bottom) experimental spectra.

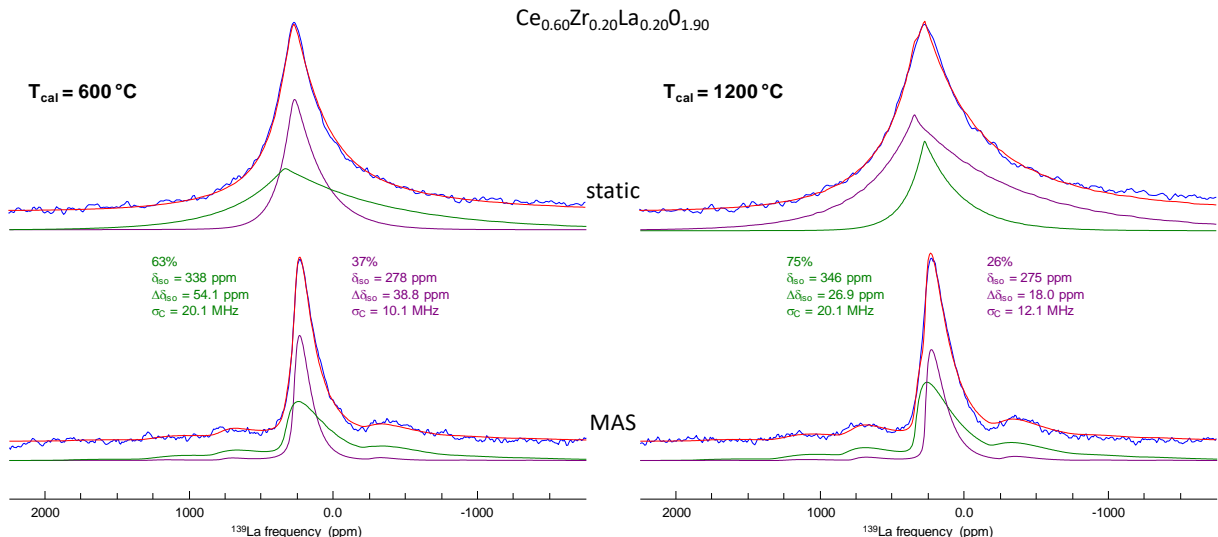


Figure 8-SI: Best fit simulations of the  $^{139}\text{La}$  NMR spectra of  $\text{Ce}_{0.60}\text{Zr}_{0.20}\text{La}_{0.20}\text{O}_{1.90}$  annealed at  $600^\circ\text{C}$  (left) and  $1200^\circ\text{C}$  (right) and using two Czjzek-like components. Simulations account simultaneously for the static (top) and spinning (bottom) experimental spectra.

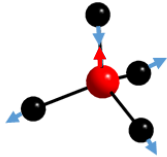
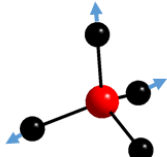
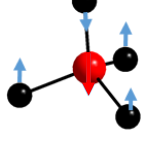
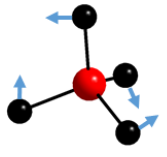
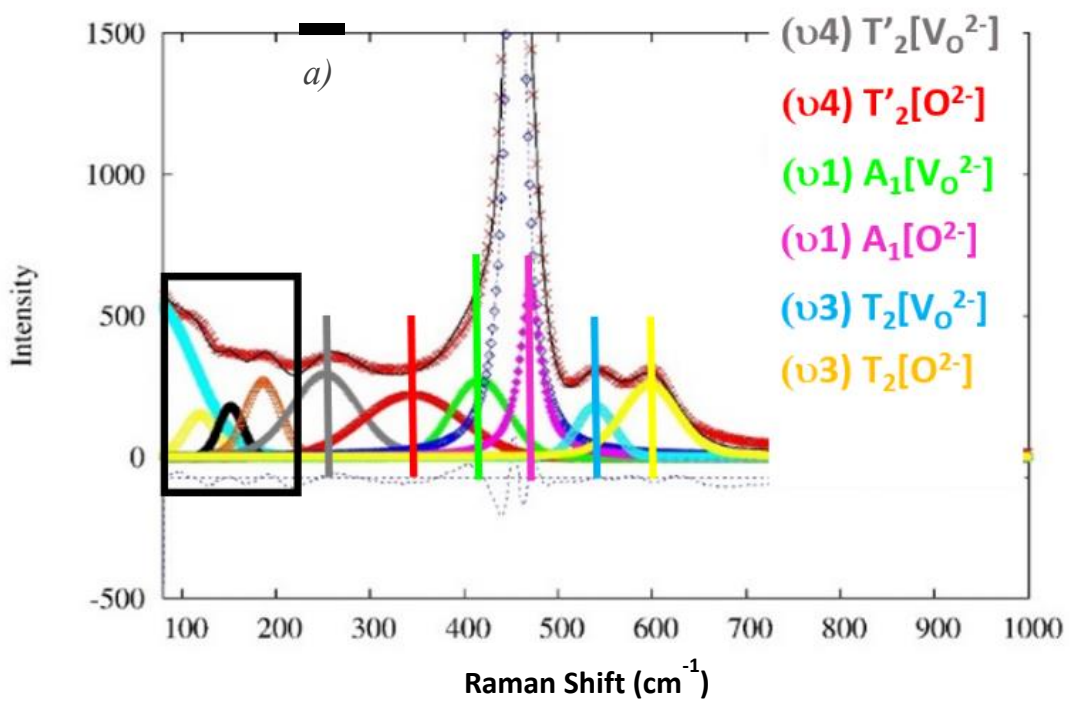
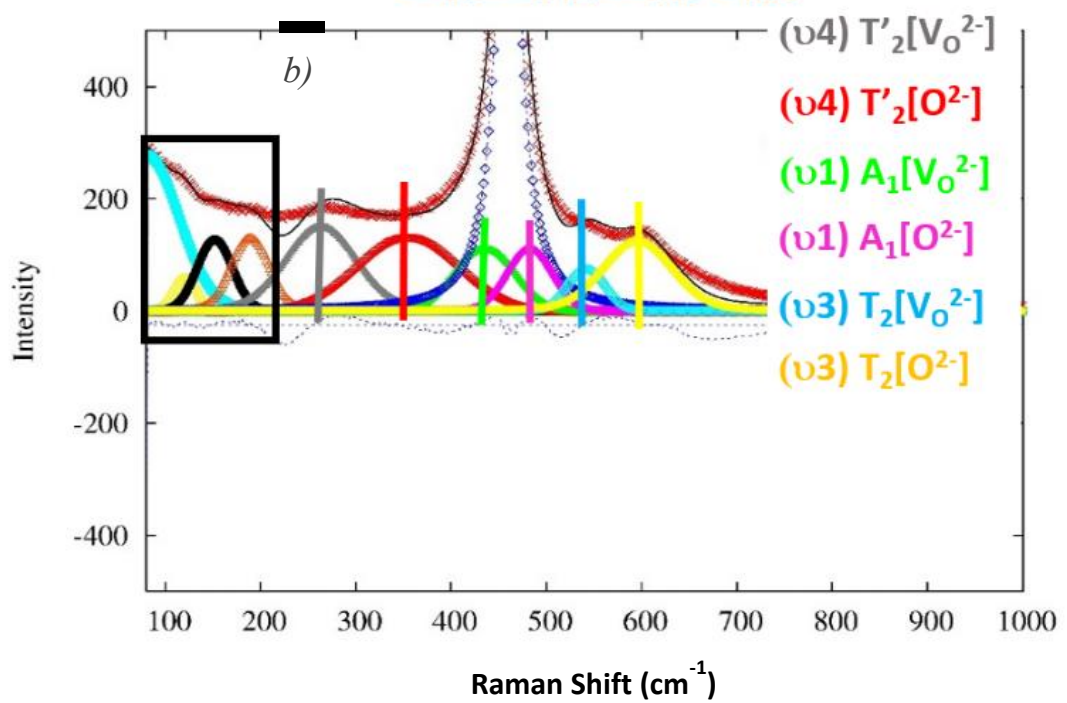
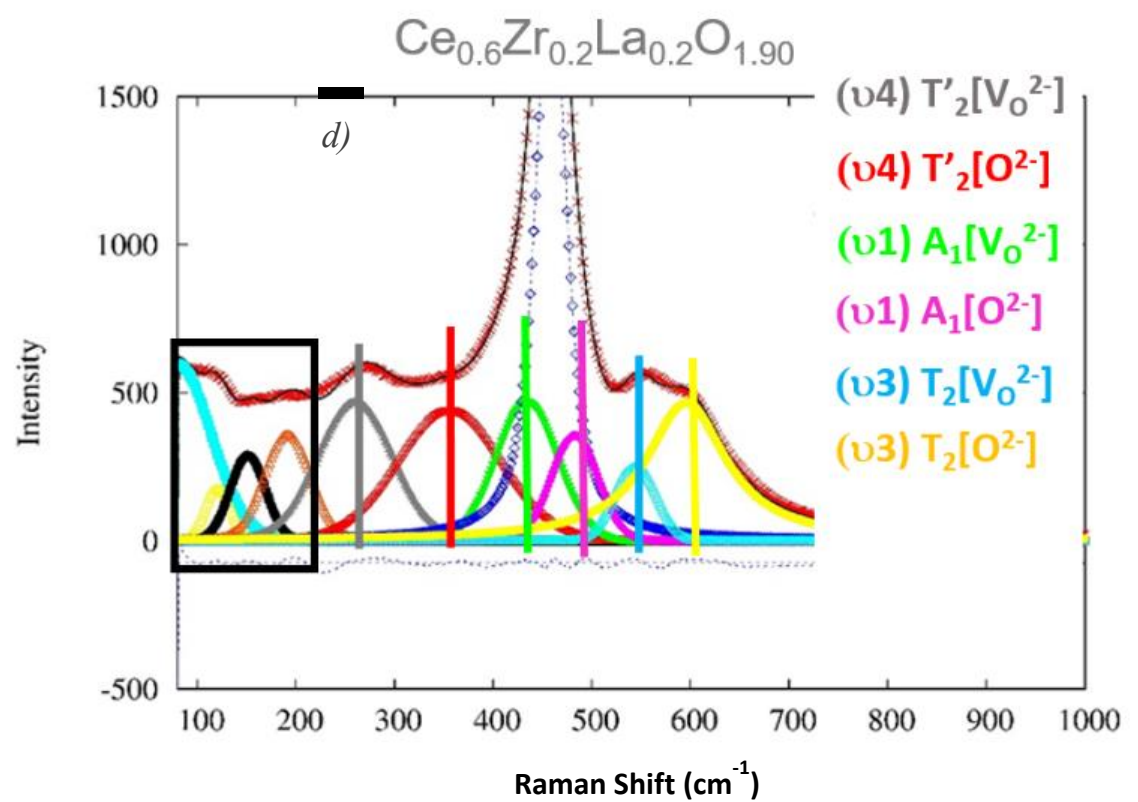
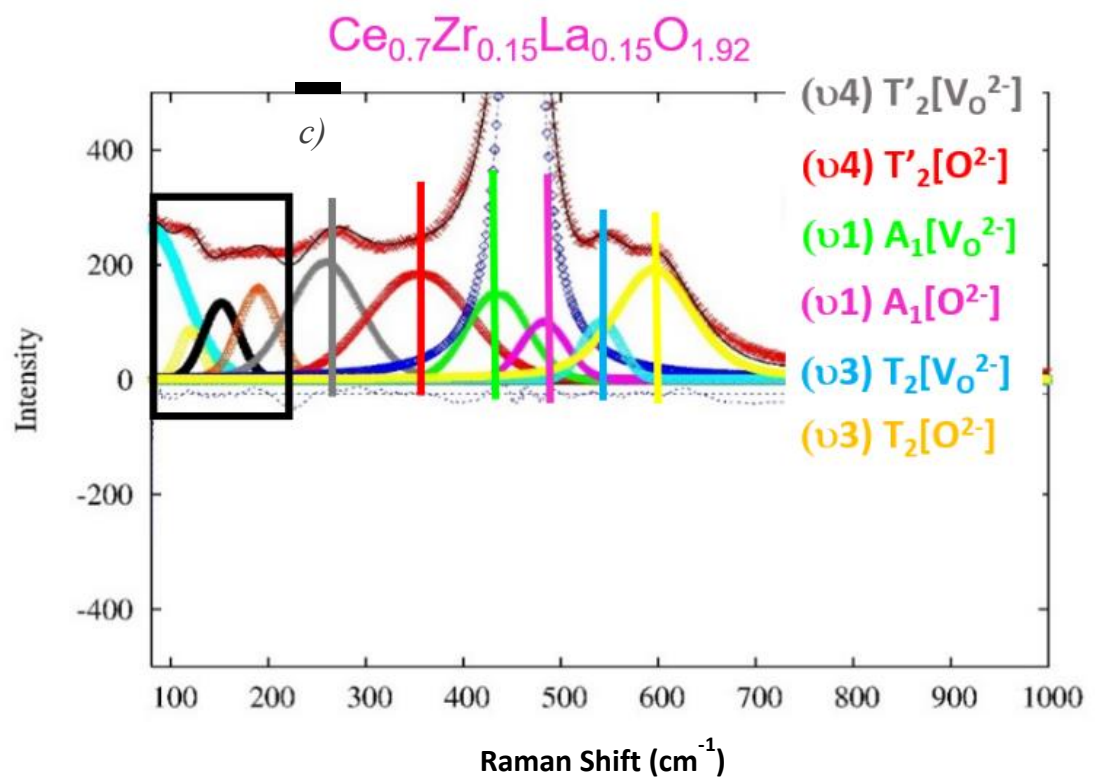
	New assignment proposal $\nu_3 > \nu_1 > \nu_4 > \nu_2$ (Nakamoto)
	<b>T<sub>2</sub> (<math>\nu_3</math>)</b> Antisymmetric $\sim 600\text{ cm}^{-1}$ <i>polar, very sensitive to charge defects (coupled with <math>\nu_4</math>)</i>
	<b>A<sub>1</sub> (<math>\nu_1</math>)</b> Symmetric $\sim 400\text{-}500\text{ cm}^{-1}$ <i>apolar, less sensitive to charge defects</i>
	<b>T<sub>2</sub> (<math>\nu_4</math>)</b> Deformation (« umbrella ») $\sim 200\text{-}300\text{ cm}^{-1}$ <i>polar, very sensitive to charge defects (coupled with <math>\nu_3</math>)</i>
	<b>E (<math>\nu_2</math>)</b> Shearing $\sim 100\text{-}200\text{ cm}^{-1}$ <i>apolar, less sensitive to charge defects</i>

Figure 9-SI : Schematic representation of various valence and deformation vibration mode of Td site, following the frequency order proposed by Nakamoto.<sup>45</sup>

$\text{Ce}_{0.9}\text{La}_{0.1}\text{O}_{1.95}$  $\text{Ce}_{0.8}\text{Zr}_{0.12}\text{La}_{0.08}\text{O}_{1.96}$ 



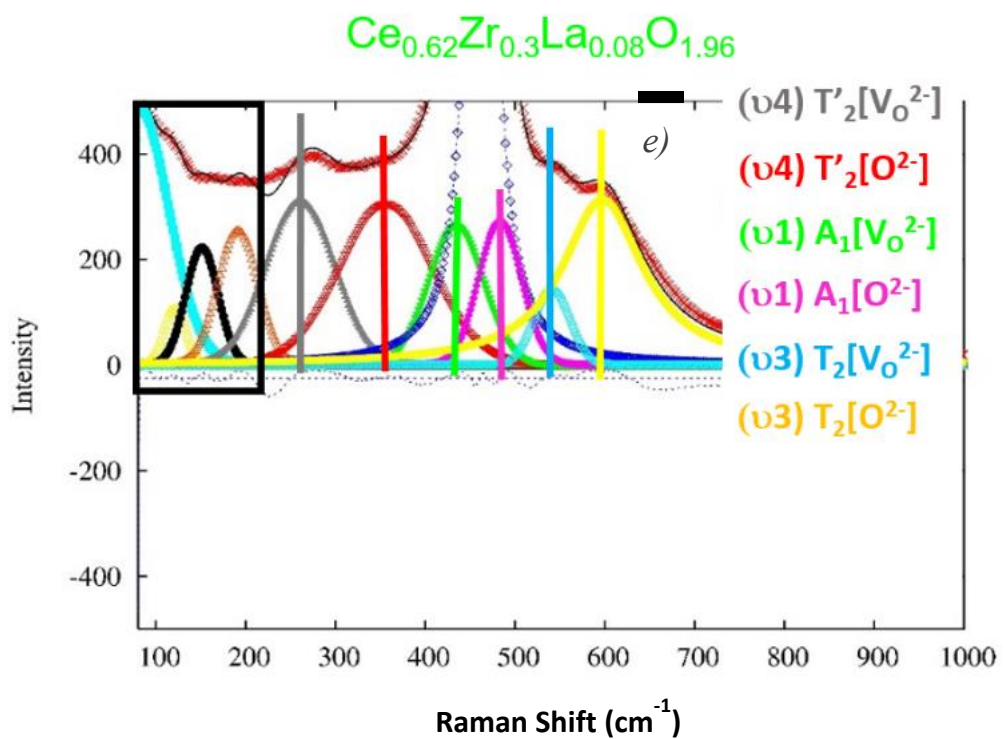
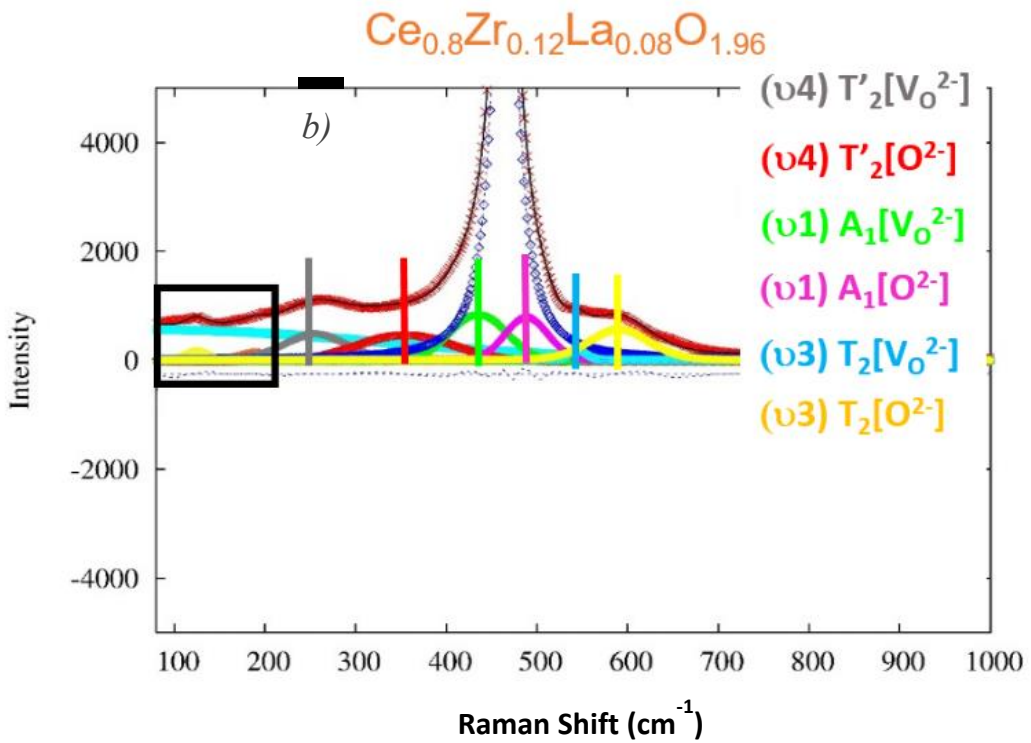
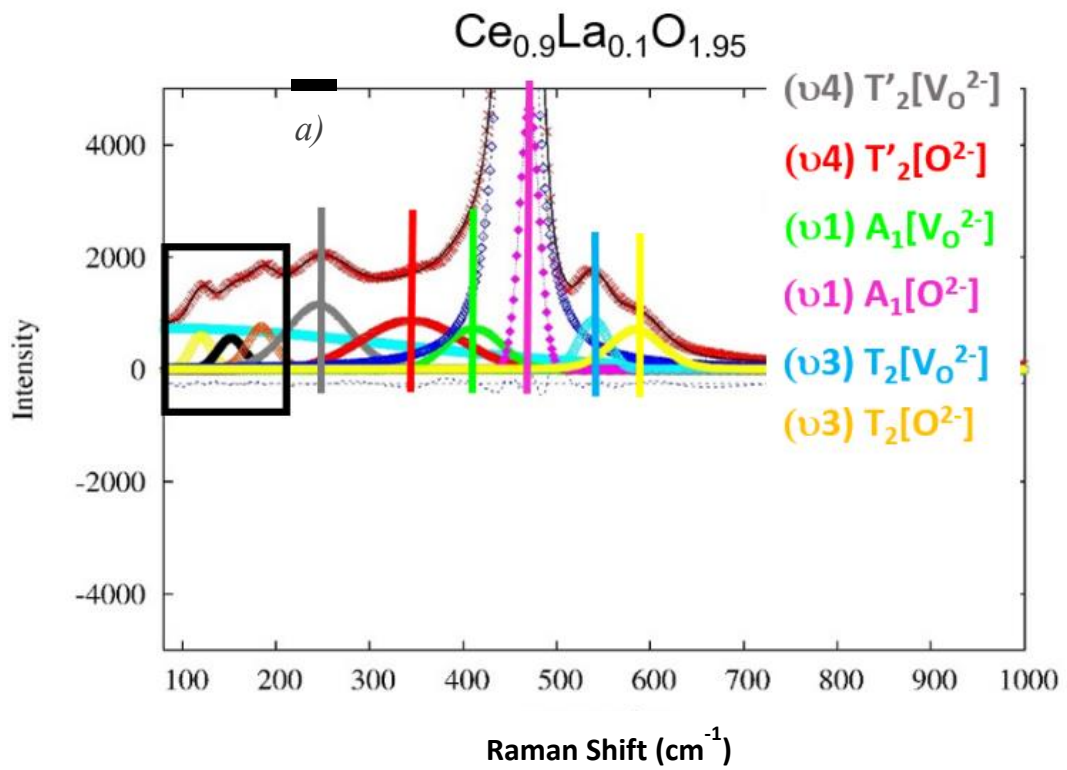


Figure 10-SI: Raman spectra deconvolution of  $\text{Ce}_{1-x-y}\text{Zr}_x\text{La}_y\text{O}_{2-z}$  complex oxides annealed at  $600^\circ\text{C}$



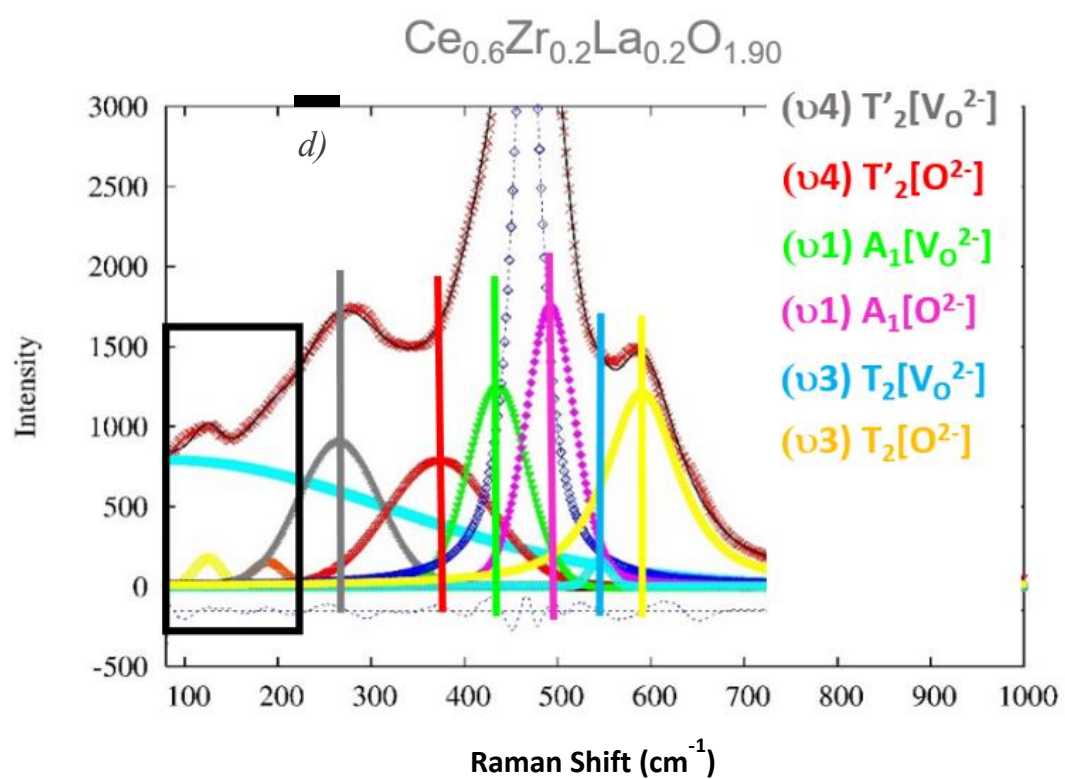
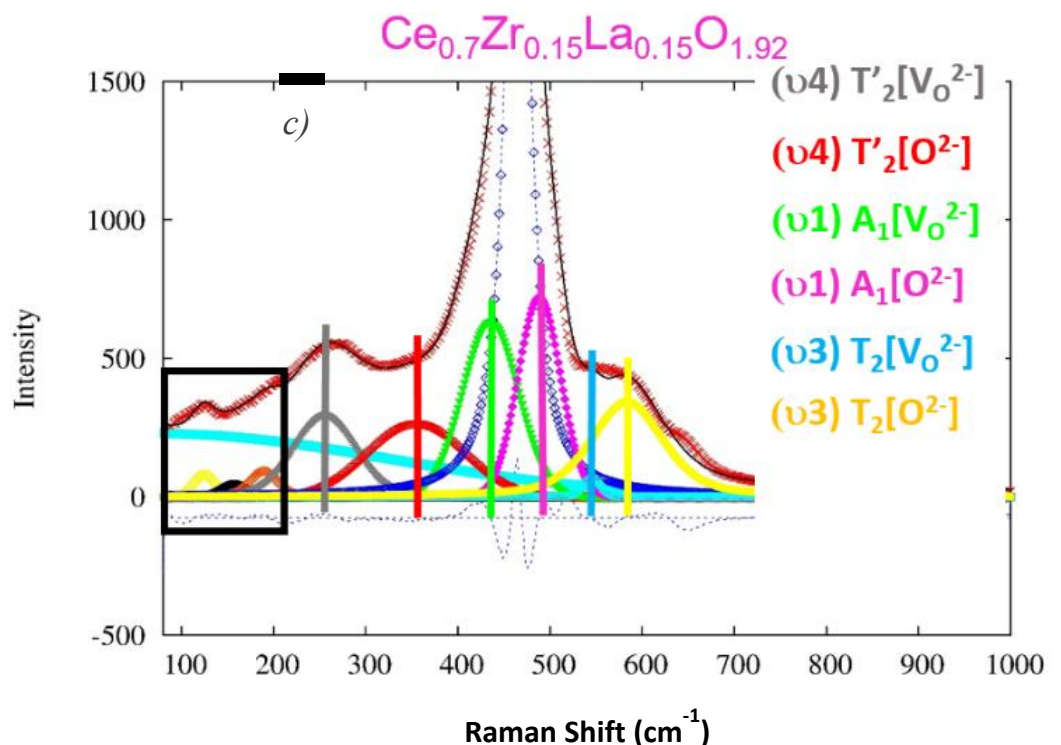


Figure 11-SI: Raman spectra deconvolution of  $\text{Ce}_{1-x-y}\text{Zr}_x\text{La}_y\text{O}_{2-z}$  complex oxides annealed at  $1200^\circ\text{C}$

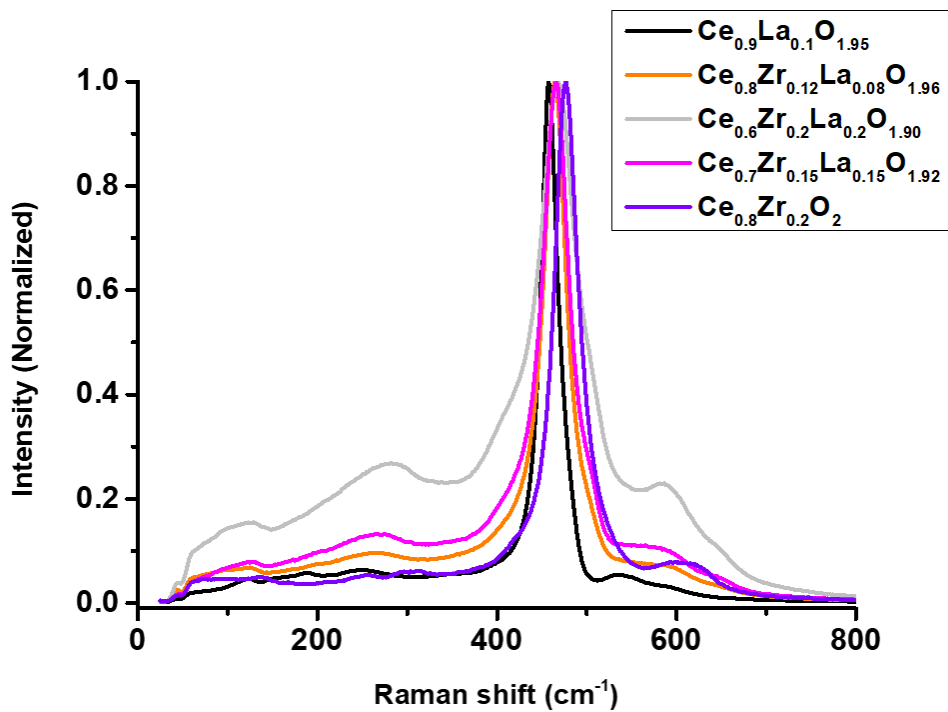


Figure 12-SI: Raman spectra of  $Ce_{1-x-y}Zr_xLa_yO_{2-z}$  complex oxides annealed at  $1200^\circ C$

## TABLE CAPTION

Table 1-SI : Elemental analysis obtained by ICP-OES

Theoretical compositions	%at. Ce	%at. Zr	%at. La
$Ce_{0.9}La_{0.1}O_{1.95}$	89	-	11
$Ce_{0.8}Zr_{0.2}O_2$	80	20	-
$Ce_{0.8}Zr_{0.12}La_{0.08}O_{1.96}$	80	11	90
$Ce_{0.7}Zr_{0.15}La_{0.15}O_{1.92}$	71	14	15
$Ce_{0.6}Zr_{0.20}La_{0.20}O_{1.90}$	60	20	20
$Ce_{0.62}Zr_{0.30}La_{0.08}O_{1.96}$	60	32	8

Table 2-SI: Structural and textural characteristics of  $Ce_{1-x-y}Zr_xRE_yO_{2-z}$  oxides annealed at 1200°C under air

Compositions ( $T_{cal} = 1200^\circ C$ )	Cell Parameters (Å)	Crystallite size (nm)
$Ce_{0.9}La_{0.1}O_{1.95}$	5.449 (1)	97 (1)
$Ce_{0.8}Zr_{0.2}O_2$	5.367 (3)	66 (1)
$Ce_{0.8}Zr_{0.12}La_{0.08}O_{1.96}$	5.413 (1)	39 (1)
$Ce_{0.7}Zr_{0.15}La_{0.15}O_{1.92}$	5.423 (2)	36 (1)
$Ce_{0.6}Zr_{0.2}La_{0.2}O_{1.90}$	5.411 (1)	29 (1)
$Ce_{0.62}Zr_{0.3}La_{0.08}O_{1.96}$	5.346 (4)	55 (1)

Table 3-SI: Experimental  $^{139}La$  NMR Parameters of  $Ce_{1-x-y}Zr_xRE_yO_{2-z}$  complex oxides annealed at 1200°C under air.

Compositions ( $T_{cal} = 1200^\circ C$ )	% site 1	$\delta_{iso}$ 1 (ppm)	$\Delta\delta_{iso}$ 1 (ppm)	$\sigma_C$ 1 (MHz)	% site 2	$\delta_{iso}$ 2 (ppm)	$\Delta\delta_{iso}$ 2 (ppm)	$\sigma_C$ 2 (MHz)
$Ce_{0.9}La_{0.1}O_{1.95}$	-	-	-	-	100	266	33	13.1
$Ce_{0.8}Zr_{0.12}La_{0.08}O_{1.96}$	19	284	40.7	4.62	81	296	54.9	11.6
$Ce_{0.7}Zr_{0.15}La_{0.15}O_{1.92}$	27	273	33.8	9.94	73	329	33.3	18.6
$Ce_{0.6}Zr_{0.2}La_{0.2}O_{1.90}$	25	275	18.0	12.1	75	346	26.9	20.1

Table 4-SI: Experimental  $^{139}La$  NMR Parameters of  $Ce_{1-x-y}Zr_xRE_yO_{2-z}$  complex oxides with error bars.

600°C										1200°C									
site	%	$\delta_{iso}$ (ppm)	$\Delta\delta_{iso}$ (kHz)	$C_Q$ MHz	%	$\delta_{iso}$ (ppm)	$\Delta\delta_{iso}$ (kHz)	$C_Q$ MHz	site	%	$\delta_{iso}$ (ppm)	$\Delta\delta_{iso}$ (kHz)	$C_Q$ MHz	%	$\delta_{iso}$ (ppm)	$\Delta\delta_{iso}$ (kHz)	$C_Q$ MHz		
$Ce_{0.80}Zr_{0.10}La_{0.10}O_2$									$Ce_{0.80}Zr_{0.10}La_{0.10}O_2$										
La <sub>(1)</sub>	75	293	5,22	21,3		0,8	0,04	0,1	La <sub>(1)</sub>	66	293	2,92	27,2		0,4	0,13	0,1		
La <sub>(2)</sub>	25	277	3,71	8,78		0,5	0,08	0,19	La <sub>(2)</sub>	34	282	13,10	7,57		0,7	0,23	0,25		
$Ce_{0.62}Zr_{0.30}La_{0.04}Y_{0.04}O_2$						3,0	1,13	0,51	$Ce_{0.62}Zr_{0.30}La_{0.04}Y_{0.04}O_2$										
La <sub>(1)</sub>	58	324	16,29	19,4		0,7	0,24	0,3	La <sub>(1)</sub>	70	379	9,99	29,6		2,4	0,59	0,3		
La <sub>(2)</sub>	42	285	5,20	8,87					La <sub>(2)</sub>	30	302	7,93	12,5		1,4	0,74	0,5		
$Ce_{0.70}Zr_{0.19}La_{0.15}O_2$						1,1	0,35	0,2	$Ce_{0.70}Zr_{0.19}La_{0.15}O_2$										
La <sub>(1)</sub>	67	293	3,54	27,6					La <sub>(1)</sub>	73	329	4,00	37,2		1,7	0,38	0,4		

*Table 5-SI: Supplementary Experimental RAMAN Parameters extracted from spectra deconvolutions of  $Ce_{1-x-y}Zr_xRE_yO_{2-z}$  complex oxides annealed at 600°C under air.*

Compositions ( $T_{cal} = 600^\circ C$ )	$T'_2[V_O^{2-}]$		$F_{2g}$			$T_2[V_O^{2-}]$		$T_2[O^{2-}]$
	Wave number (cm <sup>-1</sup> )	Intensity	Wave number (cm <sup>-1</sup> )	Intensity	Wave number (cm <sup>-1</sup> )	Gaussian Shape (%)	Wave number (cm <sup>-1</sup> )	
$Ce_{0.9}La_{0.1}O_{1.95}$	252	455	540	0.037621	97	598		
$Ce_{0.8}Zr_{0.12}La_{0.08}O_{1.96}$	263	460	542	0.015348	99	596		
$Ce_{0.7}Zr_{0.15}La_{0.15}O_{1.92}$	259	460	542	0.020556	100	596		
$Ce_{0.6}Zr_{0.20}La_{0.20}O_{1.90}$	260	458	547	0.053512	97	599		
$Ce_{0.62}Zr_{0.30}La_{0.08}O_{1.96}$	261	462	541	0.030656	97	598		

*Table 6-SI: Experimental RAMAN Parameters extracted from spectra deconvolutions of  $Ce_{1-x-y}Zr_xRE_yO_{2-z}$  complex oxides annealed at 1200°C under air.*

Compositions ( $T_{cal} = 1200^\circ C$ )	$T'_2[V_O^{2-}]$		$F_{2g}$			$T_2[V_O^{2-}]$		$T_2[O^{2-}]$
	Wave number (cm <sup>-1</sup> )	Intensity	Wave number (cm <sup>-1</sup> )	Intensity	Wave number (cm <sup>-1</sup> )	Gaussian Shape (%)	Wave number (cm <sup>-1</sup> )	
$Ce_{0.9}La_{0.1}O_{1.95}$	245	457	540	0.14327	90	585		
$Ce_{0.8}Zr_{0.12}La_{0.08}O_{1.96}$	255	458	568	0.019787	99	636		
$Ce_{0.7}Zr_{0.15}La_{0.15}O_{1.92}$	255	464	545	0.007307	95	584		
$Ce_{0.6}Zr_{0.2}La_{0.2}O_{1.90}$	265	467	545	0.020298	93	590		

*Table 7-SI: Supplementary Experimental RAMAN Parameters extracted from spectra deconvolutions of  $Ce_{1-x-y}Zr_xRE_yO_{2-z}$  complex oxides annealed at 1200°C under air.*

Compositions ( $T_{cal} = 1200^\circ C$ )	$F_{2g}$		$T_2[O^{2-}]$		$N$	$N_{La}$
	Intensity (a.u.)	Intensity (a.u.)	Gaussian Shape (%)	$N = \frac{T_2[O^{2-}]}{F_{2g}}$	$N_{La} = \frac{N}{x_{La}}$	
$Ce_{0.9}La_{0.1}O_{1.95}$	8.2837	0.28672	62	0.0346	0.3460	
$Ce_{0.8}Zr_{0.12}La_{0.08}O_{1.96}$	3.8858	0.26876	62	0.0692	0.8650	
$Ce_{0.7}Zr_{0.15}La_{0.15}O_{1.92}$	1.1623	0.27344	28	0.2308	1.5387	
$Ce_{0.6}Zr_{0.20}La_{0.20}O_{1.90}$	1.9758	1.2984	0	0.6571	3.2855	